73th International Astronautical Congress, Paris, France, 18-22 September 2022.

IAC–22–A6.IPB.2x73592

A MULTI-FIDELITY AND MULTI-DISCIPLINARY APPROACH FOR THE ACCURATE SIMULATION OF ATMOSPHERIC RE-ENTRY

Sai Abhishek Peddakotla
University of Strathclyde, Glasgow, UK, sai.peddakotla@strath.ac.uk

Fábio Morgado
University of Strathclyde, Glasgow, UK, fabio.pereira-morgado@strath.ac.uk

Dilaksan Thillaithevan
Imperial College London, United Kingdom, d.thillaithevan18@imperial.ac.uk

Danielle O'Driscoll
Imperial College London, United Kingdom, danielle.odriscoll13@imperial.ac.uk

Matthew Santer
Imperial College London, United Kingdom, m.santer@imperial.ac.uk

Christie Maddock
University of Strathclyde, Glasgow, UK, christie.maddock@strath.ac.uk

Massimiliano Vasile
University of Strathclyde, Glasgow, UK, massimiliano.vasile@strath.ac.uk

Marco Fossati*
University of Strathclyde, Glasgow, UK, marco.fossati@strath.ac.uk

Abstract

This paper proposes a multi-fidelity and multi-disciplinary framework that combines low- and high-fidelity aerothermodynamics, thermal analysis, flight dynamics, and structural analysis in a modular approach to achieve a favourable trade-off between cost and accuracy. The novelty in the current study is two-fold: one is to simulate a more accurate destructive re-entry process over using a prescribed altitude trigger for fragmentation, and the other is to implement automatic fidelity switches between high- and low-fidelity models for the aerothermodynamics based on the shock-envelope approximation of Billig's formulation. For the high-fidelity flow modelling, the open-source SU2-NEMO code is used to solve the slip to continuum regimes while the SPARTA-DSMC solver is used for transitional and free-molecular regimes. To estimate the fragmentation altitude, a linear structural analysis of objects modelled as joints are continually carried out using the FEniCS finite elements solver. A temperature-dependent von Mises yield criterion is used to identify failure in joints. The software framework, TITAN Transatmospheric Flight Simulation, is applied to the ESA ATV re-entry and fragmentation test case.
Keywords: Atmospheric Re-entry, Fragmentation, Multi-fidelity, Design for Demise, Space Debris, Fragmentation

1. Introduction

The increasing number of artificial satellites and spent rocket bodies around the Earth's orbit threatens space sustainability. They must be disposed of after reaching the end of their useful life to prevent cluttering space and reduce the chance of in-orbit collisions. A feasible solution to this problem is to subject the satellites to a destructive atmospheric re-entry, controlled or uncontrolled, during which the satellite breaks up into multiple fragments. The complete disintegration of these fragments is essential to ensure negligible risk due to surviving fragments. The debris mitigation requirements state that there must be less than 1 in 10^4 (casualty risk) [1] chance of someone being injured by surviving space debris. As a result, accurately predicting this destructive process is essential to correctly assess the ground impact risks of surviving fragments. However, the accurate prediction of re-entering fragments is a demanding and challenging task in itself, as it entails addressing a complex multi-physics problem

that includes heat transfer calculations, aerodynamic and aerothermodynamic load computations for different flow regimes, and structural dynamics and fragmentation analysis.

A re-entering object undergoes varying degrees of flow rarefaction that can be modelled successfully using high-fidelity techniques such as CFD and DSMC when applied to the appropriate flow regime. However, these high-fidelity simulations are computationally intensive, with progressively complex assumptions proportional to the growing number of fragments during the fragmentation process. This complexity and computational expense make the low-fidelity flow modelling techniques more appealing to broader usage. To address the multidisciplinary simulation requirements several re-entry tools have been created, including SCARAB (ESA/HTG) [2], PAMPERO (CNES) [3] and MUSIC/FAST (ONERA) [4]. These tools use hypersonic local panel inclination methods for the continuum regime based on modified Newtonian theory [5]. For the free-molecular regime, they use analytical approaches based on the Schaaf and Chambre flat plate model [6]. A bridging function that connects the continuum to the free molecular regime is used to obtain the necessary loads in the transitional regime [7].

Most re-entry tools use low-fidelity methods that are conservative; however, these are associated with a high degree of uncertainty arising from the simplified physical, thermo-structural assumptions and the treatment of the objects' computational geometry. There is also a growing necessity to accurately model the fragmentation process during re-entry [8, 9] owing to the use of various materials. Existing object-oriented re-entry analysis tools only use melt-based demise mechanisms and ignore destruction due to mechanical forces owing to modelling complexity. Structural fragmentation becomes relevant at temperatures close to melting as the material fails at relatively low loading conditions [8, 10]. Furthermore, most currently available low-fidelity approaches do not account for the influence of shock-generated flow characteristics and shock impingement in the dynamics and fragmentation of bodies [11], increasing simulation uncertainty.

A novel multi-fidelity-based approach is proposed using the TITAN multi-disciplinary tool [12, 13] to capture complex flow features such as shock-shock interactions and the shock-surface interactions, influencing the localised aerothermodynamic loads during hypersonic reentry. The high-fidelity solvers SU2-NEMO [14], for the continuum and slip regimes, and the SPARTA [15] (Stochastic PArallel Rarefied-gas Time-accurate Analyzer) Direct Simulation Monte Carlo (DSMC) solver, for the transitional and rarefied regimes, are used to reduce the uncertainty in the simulation results during critical phases of reentry. The SU2-NEMO CFD solver uses automatic mesh generation and anisotropic mesh adaptation to capture the complex flow interactions sharply and accurately compute their influence on the overall simulation. Dynamic grid adaptation is also performed when SPARTA is referenced to adjust the grid cell sizes to the current density distribution. The high-fidelity finite element approach for static structural analysis using the FEniCS solver [16] is utilised in the current study to enable a more natural fragmentation process involving failure of joints.

A trade-off between high- and low-fidelity models must be achieved to perform fast re-entry simulations while ensuring a satisfactory degree of confidence in the trajectory predictions. Selecting a criterion for automatically switching between low-fidelity and high-fidelity modelling becomes critical. If too many function calls to the high-fidelity model are initiated, the overall simulation becomes computationally expensive and time-consuming. On the other hand, a reduced number of function calls may not decrease the simulation uncertainty adequately. Optimally, the high-fidelity tool should only be utilised to address the phenomena not adequately resolved by low-fidelity tools, increasing confidence in the overall simulation process.

The current research intends to develop and implement automatic switching criteria to change between low-fidelity and high-fidelity aerodynamic and aerothermodynamic models during the re-entry simulation. The proposed switch criterion focuses on increasing the simulation accuracy in the presence of multiple bodies by developing a shock envelope method derived from the work of Billig [17]. Using a shock envelope allows assessing the boundaries of the fragments generated by the fragments, which can impact the neighbour objects' dynamics. Ultimately, the developed approach increases the accuracy of the results compared to the strict use of low-fidelity models, allowing to reference high-fidelity tools in critical time intervals. Therefore, the automatic fidelity trigger reduces the number of calls of the high-fidelity tool and reduces the uncertainty related to the formation of flow features derived from shock interaction in the presence of multiple fragments. The methodology described in this paper can technically applies to all the flow regimes encountered during re-entry. However, Billig's formula does not account for the level of flow rarefaction [18], requiring the use of correction factors. Only the continuum regime is considered in the current study for demonstration and validation of the methodology.

This paper is organised as follows: Section. 2 explains the TITAN logic for calculating aerodynamic and aerothermodynamic loads and the governing equations

and physical models employed by TITAN's high- and low-fidelity approaches. Section. 3 includes a summary of the structural dynamics methodology utilised for the spacecraft's finite element modelling and the joint fragmentation approach. Section. 4 provides an overview of the development of automatic fidelity switching based on shock envelope generation. Section. 5 analyses two test case scenarios regarding the reentry of the ATV satellite: (1) a natural fragmentation of the solar panels of the ATV and a study on relevant sensitivities, and (2) an induced altitude-based fragmentation of the solar panels to showcase automatic switching criteria and its benefits. Section. 6 summarises the main results and future studies.

2. Multi-fidelity Aerothermodynamics

The present multi-fidelity framework incorporated in TITAN enables the computation of aerodynamic and aerothermodynamic loads using fast simplified engineering models and accurate high-fidelity CFD/DSMC solvers. The low-fidelity models under consideration allow for the computation of the aerodynamic and aerothermodynamic quantities at the various flow regimes encountered by the bodies during the re-entry process (e.g. rarefied, transitional, slip-flow and continuum regime) using local panel inclination method based on the Modified Newtonian Theory. Additionally, the framework can calculate and use local radius information to improve surface heating prediction.

The high-fidelity simulations are computed using the CFD solver SU2-NEMO for the continuum regime and DSMC solver SPARTA [15] for the transitional and free-molecular regime. The use of CFD solvers require the generation of a grid capable of sharply capturing the flow features inside the computational domain. Therefore, before proceeding to the flow simulation, the tool automatically generates a numerical grid used to simulate the flow around the bodies. To achieve a grid-converged solution, anisotropic grid adaptation of the volume mesh and the generation of refined prismatic boundary layers is done to enable the physical surface heating accurate computation using the CFD solver. Similarly, the use of SPARTA DSMC solver requires the generation of uniform Cartesian grids to perform particle collisions and sampling of macroscopic properties, with cell sizes that are less than that of the local mean free path. Dynamical grid adaptation is automatically set up during the simulation run to ensure local cell size requirements. The generation and manipulation of the computational domain for both CFD and DSMC solvers is performed with resource to third-party tools, referenced inside the TITAN re-entry simulation framework. The flowchart for both low-fidelity and high-fidelity aerothermodynamic computation methods is showcased in Fig. 1.

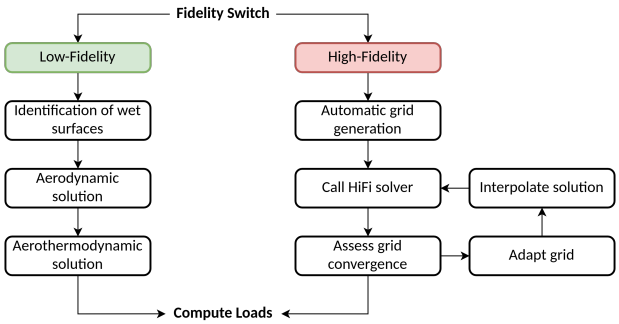

Fig. 1: Flowchart of the multi-fidelity aerothermal modelling

Although low-fidelity methods are preferable for re-entry simulations due to their low computational cost, they use simplified assumptions. Therefore, they may lead to incorrect predictions for objects with complex shapes, for flow regimes associated to high uncertainty (i.e. transitional regime), and for simulations where the presence of multiple bodies generate several shock waves that can impact the dynamics and structural integrity of neighbour objects. In these situations, the use of high-fidelity methods is advised to adequately resolve the flow conditions surrounding the objects. The implementation of an automatic switch to choose between low- and high-fidelity methods allows to reach a compromise between speed and accuracy, while allowing to appropriately resolve the scenarios that the strict use of low-fidelity models cannot. Additionally, high-fidelity methods can also be referenced to validate physical events triggered by low-fidelity models.

The multi-fidelity within TITAN is not limited to the aerodynamics and aerothermodynamic computation. In fact, TITAN also utilises a multi-fidelity approach for the computation of structural dynamics. This is achieved by the use of the third-party open-source tools FEniCS [19] and Peridigm [20], which allow the computation of the displacement and stress using a finite element and peridynamics formulation, respectively. Within the multi-fidelity approach, FEniCS is used to quickly compute the objects stress and displacement derived from the applied aerodynamic loads. If yields stress is reached and fragmentation is in imminence, Peridigm is then used to adequately verify if the applied loads are sufficient for fragmentation to occur.

2.1 SU2-NEMO

Over the years, the urging requirement to simulate chemically-reactive multi-species and non-equilibrium flows led to the development of SU2-NEMO (NonEqui-

librium MOdels solver). The closure of the governing equations for the system of interest is achieved through the linkage of SU2-NEMO and the thermochemistry library Mutation++ [21] (Multicomponent Thermodynamic And Transport properties for IONized gases in C++). The library contains efficient algorithms for the computation of the required mixture properties, such as thermodynamic, transport and chemical kinetic gas properties for a wide range of temperatures.

The system of governing equations is obtained through the extension of the Navier-Stokes equations to account for chemically-reacting, nonequilibrium flows, using the two-temperature model by Park. The translational and rotational energy mode are assumed to be at equilibrium with one another. The same approach is used for the vibrational and electronic energy mode. The system can be described as:

$$\frac{\mathrm{d}\mathbf{U}}{\mathrm{d}t} + \nabla \cdot \mathbf{F^i}(\mathbf{U}) = \nabla \cdot \mathbf{F^v}(\mathbf{U}) + \mathbf{Q}(\mathbf{U}) \qquad [1]$$

where $\mathbf{U}$ are the conservative variables, $\mathbf{Q}$ are the source terms, $\mathbf{F^i}$ and $\mathbf{F^v}$ are the inviscid and viscous fluxes, respectively. The vectors are given by,

$$\mathbf{U} = \begin{Bmatrix} \rho_1 \\ \vdots \\ \rho_{n_s} \\ \rho\mathbf{u} \\ \rho e \\ \rho e^{\text{v-e}} \end{Bmatrix}, \quad \mathbf{F^i} = \begin{Bmatrix} \rho_1\mathbf{u} \\ \vdots \\ \rho_{n_s}\mathbf{u} \\ \rho\mathbf{u}\otimes\mathbf{u} + p\bar{I} \\ \rho\mathbf{u}h \\ \rho\mathbf{u}e^{\text{v-e}} \end{Bmatrix}$$

$$\mathbf{F^v} = \begin{Bmatrix} \mathbf{J}_1 \\ \vdots \\ \mathbf{J}_{n_s} \\ \bar{\tau} \\ \bar{\tau}\cdot\mathbf{u} + \sum_s \mathbf{J}_s h_s + \mathbf{q}^{\text{t-r}} + \mathbf{q}^{\text{v-e}} \\ \sum_s \mathbf{J}_s h_s^{\text{v-e}} + \mathbf{q}^{\text{v-e}} \end{Bmatrix}, \quad \mathbf{Q} = \begin{Bmatrix} \dot{\omega}_1 \\ \vdots \\ \dot{\omega}_{n_s} \\ 0 \\ 0 \\ \dot{\Omega} \end{Bmatrix} \qquad [2]$$

in which ρ is the density, $\mathbf{u}$ is the velocity vector, p is the static pressure, h is the total enthalpy per unit mass of the mixture, e is the energy per unit mass, $\bar{\tau}$ is the viscous stress tensor, $\mathbf{q}$ is the conduction heat flux, $\mathbf{J}$ is the mass diffusion flux, $\dot{\omega}$ is the net rate of species production, $\dot{\Omega}$ is the source term of vibrational energy and n_s is the number of species in the mixture. The subscript index s stands for the s^{th} chemical species in the mixture and the superscript t-r and v-e stand for the translational-rotational and vibrational-electronic modes, respectively. If the quantity does not have a superscript, it is related to the full mixture. The term $\bar{I}$ denotes the identity matrix.

2.2 SPARTA-DSMC

Sandia's open-source parallel Direct Simulation Monte Carlo (DSMC) [22] code SPARTA [15] is used in TITAN to account for high-fidelity simulations in the transitional and rarefied regime. SPARTA discretises the computational domain into a hierarchical, multi-level Cartesian grid which is used to track simulated molecules, perform collisions and chemistry operations. Dynamic grid adaptation based on the local flow properties can be performed to improve the simulation accuracy while reducing the computational cost. The variable-hard-sphere (VHS) or the variable-soft-sphere (VSS) [22] interaction model is used to model binary collisions between the molecules while the Larsen-Borgnakke model is used to model the energy exchange between internal modes of the molecule. During particle collisions, gas-phase chemical reactions can be carried out using Bird's Total Collision Energy (TCE) [23] or Quantum-Kinetic (QK) models [24]. The gas-surface interactions (GSI) are modelled using Maxwell or the Cercignani-Lampis-Lord model (CLL) [25] that use accommodation coefficients as inputs.

The multi-fidelity methodology in TITAN can automatically create the input script that can be utilised to run high-fidelity SPARTA-DSMC simulations for specific flow conditions during the re-entry trajectory. These simulations can be computationally expensive and should be used optimally. It is important to note that one of the current study's key research contribution is the application of switching criteria based on Billig's empirical expression to predict the shape and position of shock waves. As previously stated, this expression does not account for rarefaction effects when predicting diffused shock waves in rarefied hypersonic flows [26]. It has already been established that rarefaction effects cause the shock wave's position to deviate significantly [18] from that predicted by Billig's empirical formula. Therefore, the automatic fidelity switching criteria for rarefied hypersonic flows is beyond the scope of the current study and will be investigated in a future study.

2.3 Low-fidelity models

The low-fidelity aerodynamic and aerothermodynamic models use the local panel inclination methods for hypersonic flow, enabling a rapid computation of the loads applied to the multiple fragments during atmospheric reentry. The aerodynamics in the continuum regime ($K_n \leq 10^{-3}$) is estimated with the Modified Newtonian Theory [5] while for the free-molecular regime ($K_n \geq 10^2$) it is computed using the Schaaf and Chambre [6] model for an inclined flat-plate. The pressure and shear stress contributions from each of the facets are computed as a function of local flow inclination angle (θ). Additionally, the shear

stress contribution in the continuum regime is considered to be negligible.

For the aerothermal heating estimation in the continuum regime, several analytical heat transfer correlation models like Fay-Riddell [27], Kemp-Detra-Riddell [28] and Van Driest model [29] are employed, enabling the assumption for both non-catalytic and fully-catalytic wall boundary conditions. For the rarefied regime, Schaaf and Chambre flat plate theory is used. A local radius formulation is used to increase the accuracy of the aerothermodynamics computation of blunt nosed and sharp-edged bodies.

In the transitional regime, the aerodynamics is estimated through the use of generalized aerodynamic bridging functions as described in [12, 13]. For the calculation of the aerothermodynamic properties in the transitional regime, a dedicated bridging model similar to the model developed in [30] has been integrated into TITAN. The integrated bridging function was developed using different re-entry heating data with distinct local nose radius to shift from a radius/inclination-based model in the near-continuum regime to a pure inclination-based model in the free-molecular regime. The reason being that, in the continuum regime, the heat flux is computed as a function of the local radius and panel inclination, while in the free-molecular regime, the thermal computation is radius independent.

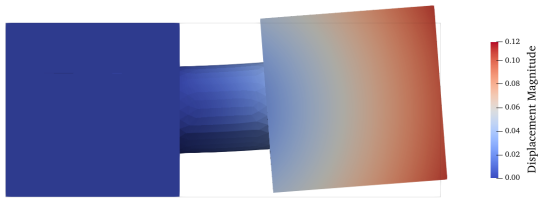

(a) 1st displacement solution

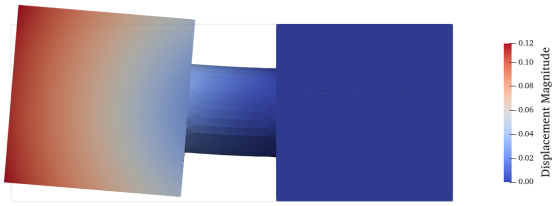

(b) 2nd displacement solution

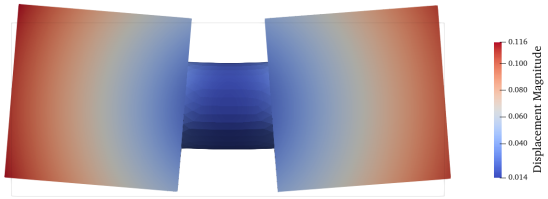

(c) Superimposed displacement

Fig. 2: Subdomain marking and displacement solutions

3. Overview of Structural Dynamics

The reentering spacecraft's components are assumed to exhibit linear elastic material properties which are constant with temperature variations. The governing equations for an elastic body, Ω, under a body force f is given by

$$\begin{aligned} -\nabla \cdot \boldsymbol{\sigma}(u) &= f \quad \text{in } \Omega \\ \boldsymbol{\sigma}(u) &= \lambda \operatorname{Tr}(\boldsymbol{\varepsilon}(u)) I + 2\mu \boldsymbol{\varepsilon}(u) \\ \boldsymbol{\varepsilon}(u) &= \frac{1}{2}(\nabla u + (\nabla(u))^T) \end{aligned} \quad [3]$$

where λ and μ are Lame's elasticity parameters defining the material properties of Ω, I is the identity tensor, $\boldsymbol{\sigma}$ is the stress tensor, Tr is the trace operator, $\boldsymbol{\varepsilon}$ is the symmetric strain tensor and u is the displacement vector.

To solve the system of linear elasticity equations shown above, a superposition-based boundary condition (BC) approach is utilised. Traditionally structures being simulated have attachment points which are modelled as Dirichlet BCs imposing displacement constraints on the structure which ensures a statically determinate system. However, as this work concerns spacecraft in freefall there are no attachment points and so no natural boundary conditions exist. Instead, to obtain the displacement, the FEA system is solved twice using two sets of Dirichlet BCs to obtain two displacement vectors which are superimposed to obtain the overall displacement of the entire structure, which is possible since the system is assumed to be linear. To demonstrate this, a simple example geometry is shown in Figure 2 is utilised. To solve the FEA problem, the cube on the left is first constrained by imposing a zero displacement Dirichlet BC on nodes located on and within the cube. The FEA problem is solved to obtain the solution shown in Figure 2a. The same process is performed to constrain the displacements on the right cube to obtain the displacement field shown in 2b. These two solutions are then superimposed to determine the total displacements over the entire structure.

To determine when fragmentation occurs, the displacement solution is used to compute the stress field on the spacecraft. In particular, the von Mises yield criterion is used to identify when yielding has occurred. In this work it is assumed that a component fragments instantaneously when the von Mises stress within a component exceeds the yield strength of its constituent material. Using the stress tensor, $\boldsymbol{\sigma}(u)$ the von Mises stress, σ_{vm} is computed

using

$$\sigma_{vm} = \sqrt{\frac{3}{2} s : s} \qquad \boldsymbol{s}(u) = \boldsymbol{\sigma}(u) - \frac{1}{3}\,\mathrm{Tr}(\boldsymbol{\sigma}(u))I \tag{4}$$

where s is the deviatronic stress tensor and fragmentation occurs when

$$\sigma_{vm} \geq \sigma_y \tag{5}$$

where σ_y is the yield stress of the material.

Structural finite element analysis (FEA) of the spacecraft are performed using the open-source partial differential equation (PDE) solver FEniCS* 2019.1.0 [19]. FEniCS has a high-level Python and C++ interface which enables a simple translation of mathematical models into finite element code. The FEniCS Python interface is utilised to allow a fast integration with TITAN, which is also implemented within Python. The library is highly flexible and supports parallel computing using MPI which enables efficient use of HPC resources making structural simulations of high-fidelity models feasible.

4. Development of a fidelity switch

The presence of neighbour objects in supersonic and hypersonic regimes can generate shock waves that have an impact on the following fragments. An example is shock impingement, where the shock impinges the surface of following bodies, leading to highly-localised aerothermal loads that impact the dynamics and the structure of the object, which cannot be fully resolved using low-fidelity methods. In order to detect if the presence of multiple bodies in the re-entry simulation give rise to such flow features that require the use of high-fidelity tools to be captured, it is necessary to estimate the shock position generated by the fragments.

There are analytical methods to estimate the shock position for simple geometries, such as tangent wedge/cone method and shock expansion theory for attached shocks [31] and Billig hyperbola formula for detached shocks [17]. However, for bodies with complex shapes, the vast majority of the methods developed for shockwave detection require the post-processing of the solution obtained from CFD/DSMC tools [32]. For re-entry simulations, the shock position has to be estimated at every time-iteration, thus the ability of quickly estimating the shock location without relying on high-fidelity tools would significantly reduce the computational cost.

Despite the fact that accurate shock estimation is difficult in the case of intricate geometries, it is possible to compute a shock envelope with a low computational cost. By definition, the shock envelope must contain the shock generated by the object itself. This approach allows to formulate a switch criteria using the relative position of the objects with respect to the shock envelope of neighbour objects. Thus, when a fragment is inside a shock envelope, high-fidelity tools are called.

This section proposes the use of Billig's formula to generate the shock envelope. An example of a similar approach was done in the work of Catalano [33], where Billig's expression was used to limit the computational domain over a Vega launcher in supersonic regime. This method assumes that the detached shockwave generated by a sphere can be written as a hyperbolic function, asymptotic to the freestream Mach angle or, in the case of a cone or wedge, to the attached shock angle θ. The expression formulated by Billig is given as

$$x = R + \Delta - R_c \cot^2\theta \left[\left(1 + \frac{r^2 \tan^2\theta}{R_c^2} \right)^{1/2} - 1 \right] \tag{6}$$

where R is the radius of curvature of the geometry at the stagnation point, R_c the radius of curvature of the shock at the vertex, Δ the stand off distance and θ the asymptotic angle of the hyperbola. The stand off distance and vertex radius of curvature are given by the empirical relation proposed in the work of Ambrosio and Wortman [34] in the continuum regime and are respectively formulated as

$$\frac{\Delta}{R} = 0.143 \exp\left(\frac{3.24}{M_\infty^2} \right) \tag{7}$$

$$\frac{R_c}{R} = 1.143 \exp\left(\frac{0.54}{(M_\infty - 1)^{1.2}} \right) \tag{8}$$

where M_∞ is the free-stream Mach number. Billig's formula is only dependent on the free-stream Mach number and the radius of the sphere, and does not take into consideration the level of flow rarefaction, as stated in the research of Nicolas et al. [18], where the authors have verified that with the increase in the Knudsen number, the stand off distance given by the empirical formula further deviates from the experimental results. Therefore, for this research, the conducted simulations are performed in the continuum regime.

The vast majority of spacecraft-oriented tools are based on low-fidelity models to conduct the simulation of the re-entry process. While TITAN enables the use of engineering models, it is not restricted to engineering methods. The multi-fidelity framework can also reference high-fidelity tools, according to the imposed level of compromise between accuracy and computational power.

An important key event in determining the dynamics of the objects is during breakup events. TITAN enables for the specification of a time window duration to run high-fidelity tools in order to assess the initial dynamics after breakup, for all the fragmentation scenarios occurring

*https://fenicsproject.org

during the re-entry process. However, the time window strategy does not allow to assess when fragments cease to be impacted by the shock generated by neighbour objects.

To account for the relative position of the bodies, an automatic fidelity switch criteria to choose between low- and high-fidelity models has been developed and integrated in the framework of TITAN, using an approach based on Billig's shock estimation for a sphere. Billig's formula enables the formulation of an analytical equation for the creation of a shock envelope, which can be used as a criteria to choose between the different fidelity methods in a fast and computationally inexpensive way. In order to generate the shock envelope using Billig's formulation, a virtual equivalent sphere needs to be considered. As an additional remark, all the procedures definitions in the following sections are performed in the wind frame, i.e., the x-axis of the referential frame is aligned with the flow.

The location of the sphere centre is computed such that the y- and z-coordinates are equal to the y- and z-coordinates of the mid-point between the maximum and minimum vertex coordinates of the object analysed. The x-coordinate of the sphere centre is equal to the minimum x-coordinate of the body. The radius of the sphere is computed such that it corresponds to the minimum radius possible to encompass the object in the y-z view plane, with the sphere centre at the already computed position. Afterwards, the shock envelope can be computed using the Billig's formula. An example of this approach is shown in Fig. 3.

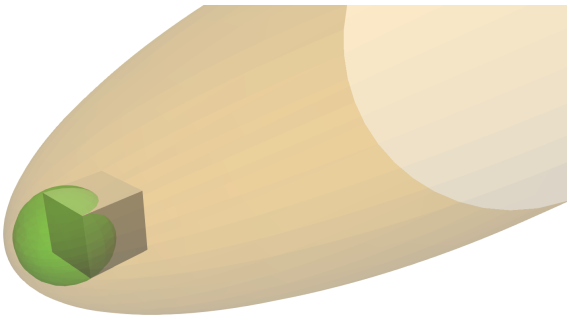

Fig. 3: Visualisation of the virtual sphere and the equivalent shock envelope for a cube geometry

The approach is tested against two cases of a Mach 10 flow, using as geometries a cube and a cylinder, which can be visualised in Fig. 4 and 5, respectively. The shock envelope generated by the equivalent sphere is able to contain the shock generated by the object for both cases, thus showcasing the capabilities of using the same formulation for complex geometries. As it can be observed for Fig. 5b, the proposed approach is conservative for elongated bodies in the y- and z- direction, while it is closely matching the shock in Fig. 5a, where the cylinder is elongated in the flow direction. This difference is due to the approach used to generate the virtual sphere, which has to include the entire object in the y-z plane perspective.

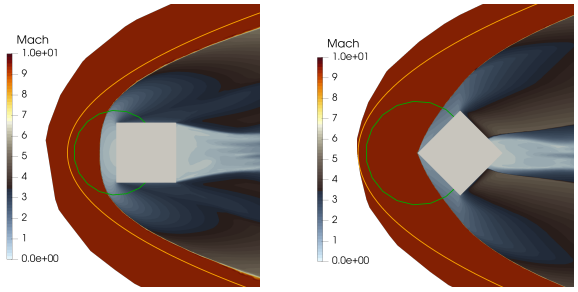

(a) Cube with 0° inclination (b) Cube with 45° inclination

Fig. 4: Shock envelope for cubic geometry at Mach 10

Due to the nature of the hyperbolic formula derived by Billig, it is possible to rewrite Eq. [6] for a sphere with an arbitrary position in the wind frame. For a body i with an equivalent sphere with centre at (x_{s_i},y_{s_i},z_{s_i}), and assuming the flow direction to be in the positive X-axis direction, the hyperbolic formula for the shock envelope can be rewritten as

$$(x - x_{s_i}) = -R_c - \Delta + R_c \cot^2\theta \left[\left(1 + \frac{(r - r_{s_i})^2 \tan^2\theta}{R_c^2} \right)^{1/2} - 1 \right] \quad [9]$$

where r is defined as

$$r = \sqrt{y^2 + z^2}. \quad [10]$$

Rearranging [11], the inner side of the hyperbola, which defines the shock envelope, can be defined as

$$R_c \cot^2\theta \left[\left(1 + \frac{(r - r_{s_i})^2 \tan^2\theta}{R_c^2} \right)^{1/2} - 1 \right] \geq -(R_c + \Delta). \quad [11]$$

For a given body j, with $i \neq j$, the coordinates of the k_{th} vertex of the body are given as (x_{j_k},y_{j_k},z_{j_k}). If any of the vertexes is inside the hyperbola, CFD tools are used to compute the aerothermal loads. Otherwise, if all the vertex are outside the hyperbola, low-fidelity methods are used. In other words, high-fidelity methods are used if a single vertex complies with the following criteria:

$$(x_{j_k} - x_{s_i}) - R_c \cot^2\theta \left[\left(1 + \frac{(r_{j_k} - r_{s_i})^2 \tan^2\theta}{R_c^2} \right)^{1/2} - 1 \right] \geq -(R_c + \Delta), \quad \text{for k = 0, 1, ..., N.} \quad [12]$$

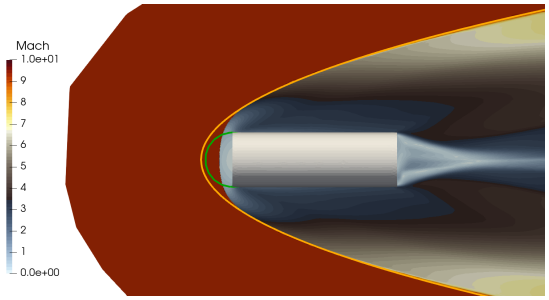

(a) Cylinder with revolution axis parallel to the flow direction

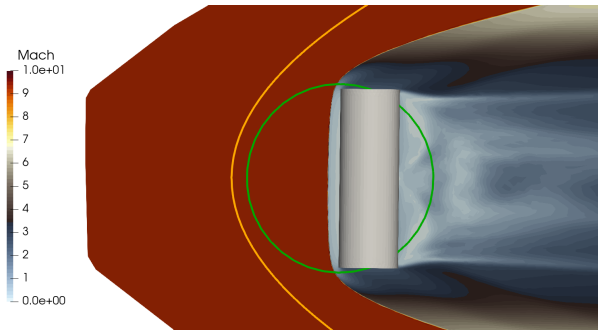

(b) Cylinder with revolution axis normal to the flow direction

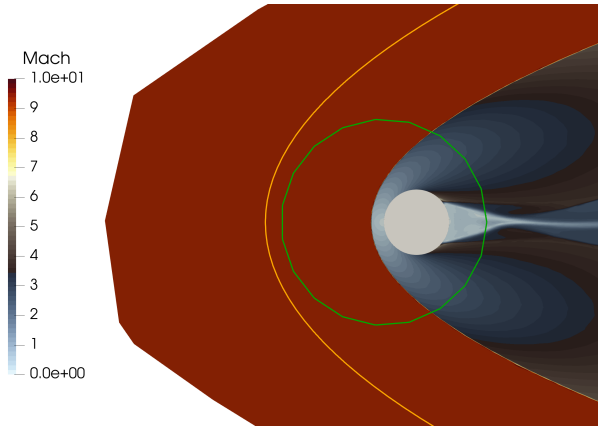

(c) Cylinder with revolution axis normal to the flow direction

Fig. 5: Shock envelope for cylindrical geometry at Mach 10

An illustrative example of the proposed methodology for the fidelity switch criteria is presented in Fig. 6, where the vertexes inside the envelope are flagged. Therefore, in this example, if any of the fore-sphere vertexes are inside the shock envelope generated by the leading sphere, high-fidelity tools are used for the computation of the surface loads. The considered approach not only allows to account for objects leaving the shock envelope, but also for fragments re-entering it, thus eventual interaction with the shock generated by a leading fragment can be expected.

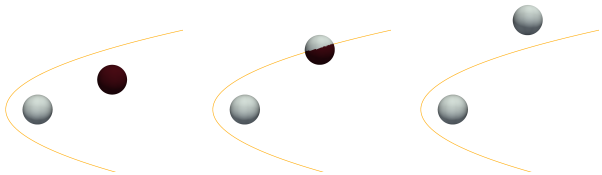

Fig. 6: Representation of the sphere positioning in relation to the shock envelope.

Some fragments may not able to leave the shock generated by the leading object, thus not leaving the shock envelope. From the methodology described so far, this would imply that the high-fidelity tools would be referenced at every time iteration, leading to high computational costs. To prevent this, it is important to enclose the shock envelope longitudinally, but the selection for the enclosing criteria is complex and subject to future research. For this work, only the envelope criteria generated by Billig's formula is considered.

5. ATV satellite re-entry

5.1 Automatic fidelity switching

In order to demonstrate the multi-fidelity capabilities of TITAN with the automatic fidelity switch presented in this work and assess its impact on the dynamics of the fragments, a conceptual ATV re-entry test-case without thermal ablation was conducted. A previously conducted work [12] has already demonstrated the existence of discrepancies between high-fidelity and low-fidelity methods instants after the fragmentation of the joints connecting the main body and the solar panels due to shock influence. The initial trajectory conditions and fragmentation trigger used in this simulation are summarised in Table 1 and the initial simplified ATV geometry before the breakup is shown in Fig. 7.

Table 1: Initial trajectory conditions and geometry details

Parameter	Value
Altitude [km]	120
Velocity [km/s]	7.57
Flight path angle [°]	-1.45
Initial pitch angle velocity [°/s]	10
Fragmentation trigger altitude [km]	78
Number of facets [$\times 10^3$]	40
Time step [s]	0.25

Up until the moment of fragmentation at 78 km, TITAN uses low-fidelity models to compute the surface

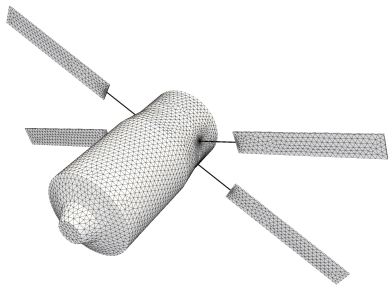

Fig. 7: Geometry configuration of the conceptual ATV geometry.

loads. The ATV trajectory up until fragmentation can be visualised in Fig. 8.

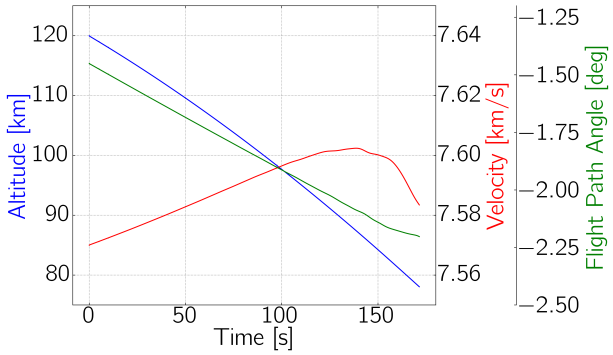

Fig. 8: ATV trajectory profile before breakup.

At the moment of fragmentation ($t = 171.95$ s), the objects are re-entering at Mach 26, leading to the formation of shock-waves. Using the methodology described in Section **??**, it is possible to estimate if the fragments are subjected to the influence of the shock generated by leading objects, requiring the use of high fidelity methods for accurate predictions of surface loads. The forces and moments applied to the fragments were computed for a time interval of $\Delta t = 2.0$ s using a time step of $dt = 0.05$ s for both low- and high-fidelity methods to compare the differences.

The results shown in Fig. 9 illustrate the forces and moments experienced by a single solar panel. The plots show results for both low and high-fidelity models. The blue background indicates the time interval where the fragment is inside a shock envelope generated by the main body or leading panels, thus requiring the use of high-fidelity tools, and the yellow background indicates the time interval where the fragment is not interacting with any shock envelope, thus low-fidelity models can be used. As it can be verified, the difference in the methods is more pronounced when the fragment is inside the shock envelope due to the influence of the leading body. As the fragment leaves the shock envelope, the forces and moments computed using both methods become comparable as there is no further interaction with shock waves. Therefore, after exiting the envelope, low-fidelity methods are enough to capture the object's dynamics adequately.

Three different scenarios were sequentially identified in Fig. 9 by a black dashed line. After fragmentation of the joints, due to the proximity of the solar panels and the main body, high-fidelity methods are required to fully capture the loads applied in the fragments, as visualised in Fig. 10. Afterwards, the tracked solar panel leaves the shock influence of the remaining fragments. At this stage, TITAN is able to separate the fragments whose dynamics can be captured using Modified Newtonian from the fragments that require the generation of a numerical grid to run a CFD/DSMC simulation. The fragment selection process enables to reduce the number of objects in the high-fidelity simulation, thus minimising the computational cost. This scenario, illustrated in Fig. 11, is similar to the one represented by the yellow background, where the forces and moments using both low and high fidelity are in good agreement.

Lastly, a scenario was observed where different clusters of fragments were not interacting with other clusters, but the shock influence was noticeable inside both clusters, requiring the use of high-fidelity models. TITAN can separate the fragments that are interacting with each other into separate clusters according to the generated shock envelope . Therefore, the shock-waves generated from the fragments associated to a cluster do not interact with other clusters, as it can be verified in Fig. 12, TITAN is able to run separate high-fidelity simulations, reducing the time and complexity of the flow computation. The panel used for the comparison in Fig. 9 is circled in red.

The proposed conservative method ensures that the objects outside the shock envelope hyperbola do not interact with leading shocks. Therefore, it is expected for the forces and moments computed by both CFD and Modified Newtonian method to be similar. The use of an analytical function to assess the position of the objects with respect to the generated shock envelops allows to quickly assess the level of fidelity required to adequately compute the applied loads at the given instant of time.

5.2 Fragmentation due to mechanical loads

6. Conclusions

The current study aims to investigate an automatic fidelity switching criteria based on the creation of a shock envelope. Billig's empirical shock relation for a sphere is used to generate equivalent shock envelopes for various primitive objects to aid the development of a fidelity

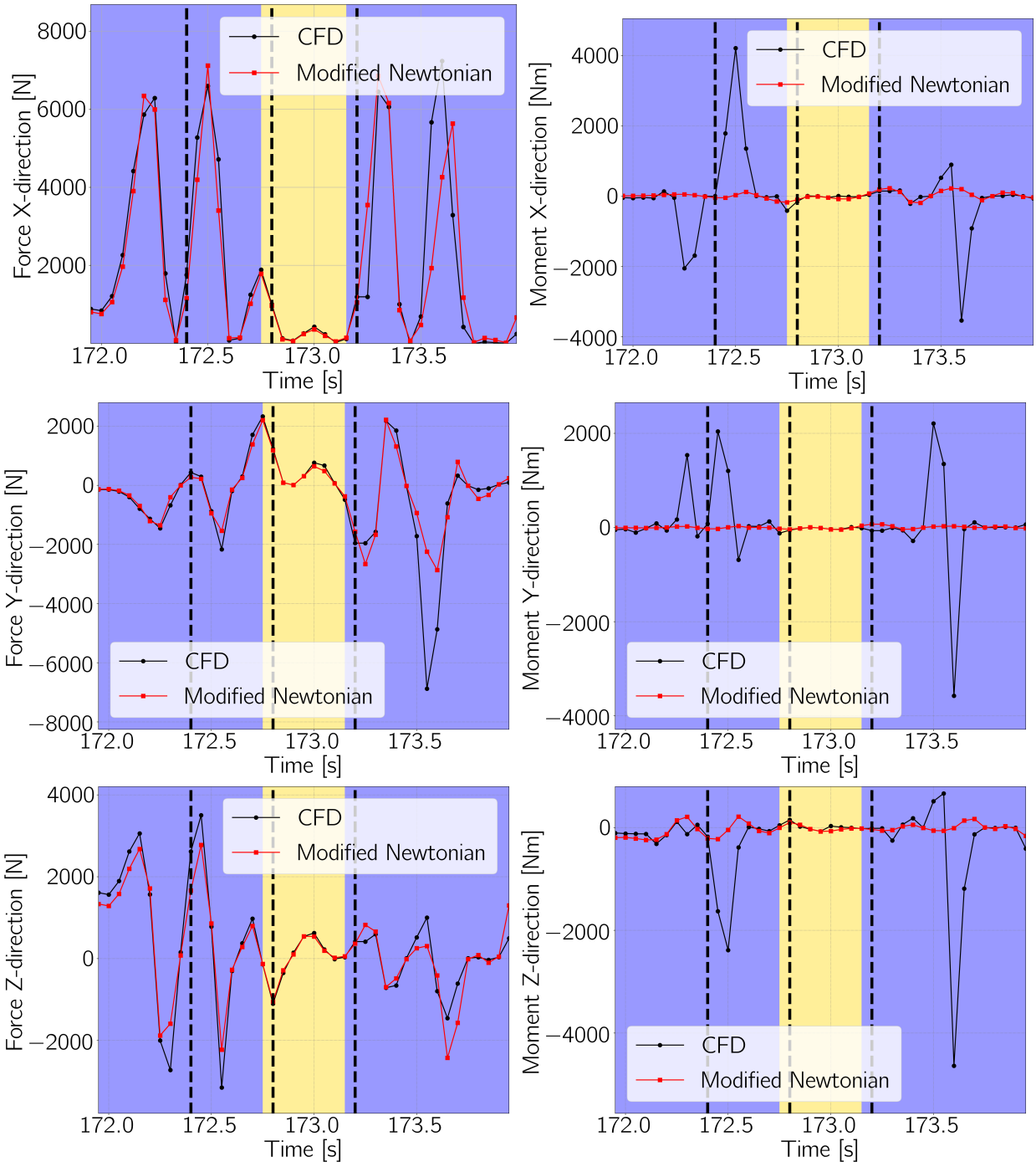

Fig. 9: Solar panel forces and moments comparison.

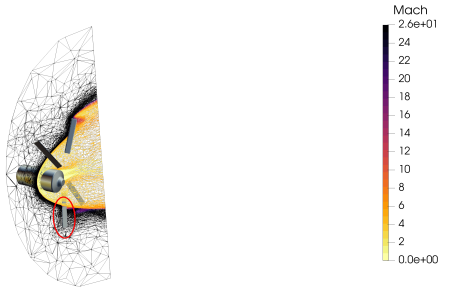

Fig. 10: Full CFD simulation at $t = 172.4s$ using one cluster

Fig. 11: Fidelity separation at $t = 172.8s$. Low-fidelity model is used for the circled solar panel

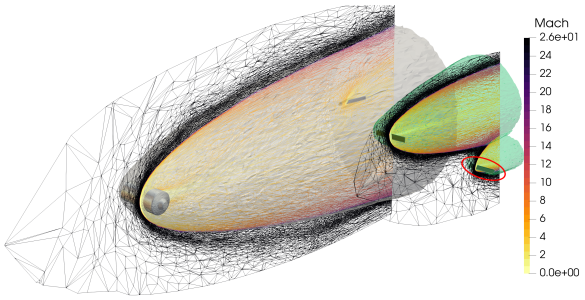

Fig. 12: Mach iso-surface for different clusters at $t = 173.3$ s

Table 2: Elevated temperature material properties of Al6061-T651

Temperature (^0C)	$E\ (GPa)$[35]	$\sigma_Y\ (MPa)$[35]
24	68	295
200	59	240
300	47	95
500	12	8

switch for multiple bodies simulation.

The proposed methodology allows automatic switching between the low-fidelity local-panel inclination methods and the high-fidelity Computational Fluid Dynamics or Direct Simulation Monte Carlo techniques, such that the complex flow features resulting from the proximity of the bodies are adequately resolved to increase the confidence in the simulations. A conceptual re-entry test case scenario using the Automated Transfer Vehicle geometry was used to simulate the moments after the solar panels fragment from the main body of the ATV, with a shock envelope criteria to assess the level of fidelity required at each time iteration and for each object analysed.

Acknowledgment

This research is supported by a joint collaboration between: UK Space Agency NSTP-SST-007 project, ESA MIDGARD project: ESA Contract No. 4000130436/20/NL/MH/ac (2020-2023), and EU H2020 MSCA-ETN Stardust-R: grant agreement 813644.

References

[1] J.-C. Liou, M. Kieffer, A. Drew, and A. Sweet, "The 2019 u.s. government orbital debris mitigation standard practices," *Orbital Debris Quarterly News*, vol. 24, no. 1, pp. 4–8, 2020.

[2] G. Koppenwallner, B. Fritsche, T. Lips, and H. Klinkrad, "Scarab - a multi-disciplinary code for destruction analysis of space-craft during re-entry," *European Space Agency, (Special Publication) ESA SP*, vol. 563, p. 281, 01 2005.

[3] J. Annaloro, P. Omaly, V. Rivola, and M. Spel, "Elaboration of a new spacecraft-oriented tool: Pampero," in *Proceedings of the 8th European Symposium on Aerothermodynamics for Space Vehicles*, 2015.

[4] F. Sourgen, Y. Prévereaud, J. l. Verant, E. Laroche, and J.-M. Moschetta, "Music/fast, a pre-design and pre-mission analysis tool for the earth atmospheric re-entry of spacecraft, capsules and de-orbited satellites," in *Proceedings of 8th European Symposium on Aerothermodynamics for Space Vehicles, 2 March 2015 - 6 March 2015 (Lisbonne, Portugal*, 2015.

[5] L. Lees, "Hypersonic flow," *Journal of Spacecraft and Rockets*, vol. 40, no. 5, pp. 700–735, 2003.

[6] S. A. Schaaf and P. L. Chambre, *Flow of Rarefied Gases*. Princeton University Press, 1958.

[7] L. Morsa, G. Zuppardi, A. Schettino, and R. Votta, "Analysis of bridging formulae in transitional

Table 3: Break-up altitude of solar panels with breaking stress, at a constant Young's modulus of 12.0 GPa

Breaking stress (MPa)	Demise mechanism	Break-up altitude (km)			
		Panel-1	Panel-2	Panel-3	Panel-4
1.0	Structural fragmentation	94.20	94.13	94.07	94.00
2.0	Structural fragmentation	86.22	86.15	86.08	86.01
2.5	Structural fragmentation	85.66	85.66	85.59	85.59
3.0	Thermal disintegration	85.18	85.04	85.04	86.42
8.0	Thermal disintegration	85.18	85.04	85.04	86.42

Table 4: Variation of the breakup altitude of solar panels with modulus of elasticity, at a constant breaking stress of 1.0 MPa

Young's modulus (GPa)	Demise mechanism	Break-up altitude (km)			
		Panel-1	Panel-2	Panel-3	Panel-4
12.0	Structural	94.20	94.13	94.07	94.00
10.0	Structural	94.20	94.13	94.07	94.00
8.0	Structural	94.20	94.13	94.07	94.00
6.0	Structural	94.20	94.13	94.07	94.00

regime," *AIP Conference Proceedings*, vol. 1333, 05 2011.

[8] S. A. Peddakotla, J. Yuan, E. Minisci, M. Vasile, and M. Fossati, "A numerical approach to evaluate temperature-dependent peridynamics damage model for destructive atmospheric entry of spacecraft," *The Aeronautical Journal*, pp. 1–30, 2022.

[9] S. A. Peddakotla, E. Minisci, and M. Fossati, "A novel approach for the accurate simulation of re-entry fragmentation," in *72nd International Astronautical Congress, Dubai, UAE*, 2021.

[10] J. G. Kaufman, *Properties of aluminum alloys: tensile, creep, and fatigue data at high and low temperatures*. Materials Park, OH, USA: ASM international, 1999.

[11] J. Annaloro, S. Galera, P.Kärräng, Y. Prevereaud, J.-L. Vérant, M. Spel, P. Van Hauwaert, and P. Omaly, "Space debris atmospheric entry prediction with spacecraft-oriented tools," 04 2017.

[12] F. Morgado, S. A. Peddakotla, C. Garbacz, M. L. Vasile, and M. Fossati, "Multi-fidelity approach for aerodynamic modelling and simulation of uncontrolled atmospheric destructive entry," 2022.

[13] F. Morgado, S. A. Peddakotla, and M. Fossati, "A multi-fidelity simulation framework for atmospheric re-entering bodies," in *ESA Aerothermodynamics and Design for Demise (ATD3) Workshop*, 2021.

[14] W. T. Maier, J. T. Needels, C. Garbacz, F. Morgado, J. J. Alonso, and M. Fossati, "SU2-NEMO: An Open-Source Framework for High-Mach Nonequilibrium Multi-Species Flows," *Aerospace*, vol. 8, no. 7, 2021. 10.3390/aerospace8070193.

[15] S. Plimpton, S. Moore, A. Borner, A. Stagg, T. Koehler, J. Torczynski, and M. Gallis, "Direct simulation monte carlo on petaflop supercomputers and beyond," *Physics of Fluids*, vol. 31, no. 8, p. 086101, 2019.

[16] M. Alnæs, J. Blechta, J. Hake, A. Johansson, B. Kehlet, A. Logg, C. Richardson, J. Ring, M. E. Rognes, and G. N. Wells, "The fenics project version 1.5," *Archive of Numerical Software*, vol. 3, no. 100, 2015.

[17] F. S. Billig, "Shock-wave shapes around spherical- and cylindrical-nosed bodies.," *Journal of Spacecraft and Rockets*, vol. 4, no. 6, pp. 822–823, 1967.

[18] N. Rembaut, R. Joussot, and V. Lago, "Aerodynamical behavior of spherical debris in the supersonic and rarefied wind tunnel marhy," *Journal of Space Safety Engineering*, vol. 7, no. 3, pp. 411–419, 2020. Space Debris: The State of Art.

[19] M. S. Alnæs, J. Blechta, J. Hake, A. Johansson, B. Kehlet, A. Logg, C. Richardson, J. Ring, M. E. Rognes, and G. N. Wells, "The FEniCS Project Version 1.5," *Archive of Numerical Software*, 2015.

[20] J. M. M.L. Parks, D.J. Littlewood and S. Silling, "Peridigm Users' Guide," *Sandia National Laboratories*, 2012.

[21] J. Scoggins and T. Magin, "Development of mutation++: Multicomponent thermodynamic and transport properties for ionized plasmas written in c++," 06 2014.

[22] G. Bird, *Molecular gas dynamics and direct simulation Monte Carlo*. 1998.

[23] G. Bird, "Chemical reactions in dsmc," in *AIP Conference Proceedings*, vol. 1333, pp. 1195–1202, American Institute of Physics, 2011.

[24] G. Bird, "The qk model for gas-phase chemical reaction rates," *Physics of Fluids*, vol. 23, no. 10, p. 106101, 2011.

[25] R. Lord, "Some further extensions of the cercignani–lampis gas–surface interaction model," *Physics of Fluids*, vol. 7, no. 5, pp. 1159–1161, 1995.

[26] M. Ivanov and S. Gimelshein, "Computational hypersonic rarefied flows," *Annual Review of Fluid Mechanics*, vol. 30, no. 1, pp. 469–505, 1998.

[27] J. Fay and F. R. Riddell, "Theory of stagnation point heat transfer in dissociated air," *Journal of the Aerospace Sciences*, vol. 25, pp. 73–85, 1958.

[28] R. W. Detra, "Addendum to heat transfer to satellite vehicle reentering the atmosphere," *Jet Propulsion*, vol. Dec., pp. 1256–1257, 1957.

[29] E. R. van Driest, "The problem of aerodynamic heating," *Aeronautical Engineering Review*, vol. 15, 10, pp. 26–41, 1956.

[30] A. Falchi, V. Renato, E. Minisci, and M. Vasile, "Fostrad : An advanced open source tool for reentry analysis," in *15th Reinventing Space Conference*, (GBR), October 2017.

[31] J. D. Anderson, *Hypersonic and high temperature gas dynamics*. AIAA, 2000.

[32] Z. Wu, Y. Xu, W. Wang, and R. Hu, "Review of shock wave detection method in cfd post-processing," *Chinese Journal of Aeronautics*, vol. 26, no. 3, pp. 501–513, 2013.

[33] P. Catalano, M. Marini, A. Nicolì, and A. Pizzicaroli, "Cfd contribution to the aerodynamic data set of the vega launcher," *Journal of Spacecraft and Rockets*, vol. 44, no. 1, pp. 42–51, 2007.

[34] A. Ambrosio and A. Wortman, "Stagnation-point shock-detachment distance for flow around spheres and cylinders in air," *Journal of the Aerospace Sciences*, vol. 29, no. 7, pp. 875–875, 1962.

[35] P. T. Summers, Y. Chen, C. M. Rippe, B. Allen, A. P. Mouritz, S. W. Case, and B. Y. Lattimer, "Overview of aluminum alloy mechanical properties during and after fires," *Fire Science Reviews*, vol. 4, no. 1, pp. pp. 1–36, 2015.